

---

# Large anomalous Nernst effect in the ferromagnetic Fe<sub>3</sub>Si polycrystal

Yangming Wang,<sup>1,2</sup> Susumu Minami,<sup>1</sup> Akito Sakai,<sup>1,2</sup> Taishi Chen,<sup>1,2,3</sup>

Zili Feng,<sup>1,2</sup> Daisuke Nishio-Hamane,<sup>2</sup> and Satoru Nakatsuji<sup>1,2,4,5,6,\*</sup>

<sup>1</sup>*Department of Physics, University of Tokyo, Bunkyo-ku, Tokyo 113-0033, Japan*

<sup>2</sup>*Institute for Solid State Physics, University of Tokyo, Kashiwa, Chiba 277-8581, Japan*

<sup>3</sup>*School of Physics, Southeast University, Nanjing, 211189, China*

<sup>4</sup>*Institute for Quantum Matter and Department of Physics and Astronomy,*

*Johns Hopkins University, Baltimore, Maryland 21218, USA*

<sup>5</sup>*CREST, Japan Science and Technology Agency (JST),*

*4-1-8 Honcho Kawaguchi, Saitama 332-0012, Japan*

<sup>6</sup>*Trans-scale Quantum Science Institute,*

*University of Tokyo, Bunkyo-ku, Tokyo 113-8654, Japan*

---

## Abstract

The high-throughput calculation predicts that the Fe-based cubic ferromagnet  $\text{Fe}_3\text{Si}$  may exhibit a large anomalous Nernst effect (ANE). Here, we report our experimental observation of the large Nernst coefficient  $S_{yx} \sim 2 \mu\text{V/K}$  and the transverse thermoelectric coefficient  $-\alpha_{yx} \sim 3 \text{ Am}^{-1}\text{K}^{-1}$  for  $\text{Fe}_3\text{Si}$  polycrystal at room temperature. The large  $-\alpha_{yx}$  indicates that the large ANE originates from the intrinsic Berry curvature mechanism. The high Curie temperature of 840 K and the most abundant raw elements of Fe and Si make  $\text{Fe}_3\text{Si}$  a competitive candidate for Nernst thermoelectric generations.

Keywords: Anomalous Nernst effect, Thermoelectrics, Ferromagnet, Polycrystal

## I. INTRODUCTION

The thermoelectric (TE) effect, converting the heat current into electric energy directly, has a great potential for energy harvesting and heat flow sensors for advanced Internet of Things (IoT) society [1–3]. Ferromagnets can induce transverse thermoelectric voltages, so-called anomalous Nernst effect (ANE), which appears perpendicular to heat flow and magnetization. Recently, the ANE has attracted wide attention owing to its unique advantages for large-area and flexible thermoelectric devices [4, 5]. Thanks to recent developments in topological physics, giant ANE and anomalous Hall effect (AHE) enhanced by the large Berry curvature have been discovered in various ferromagnets and even antiferromagnets [6–10]. One of the most attractive candidates is  $\text{Fe}_3X$  ( $X = \text{Ga}, \text{Al}$ ) where the Nernst coefficient  $S_{yx}$  reaches up to 6 and 4  $\mu\text{V/K}$  at room temperature in  $\text{Fe}_3\text{Ga}$  and  $\text{Fe}_3\text{Al}$ , respectively [7]. The theoretical analysis indicates that such a giant ANE originated from the topological nodal web structure around the Fermi energy  $E_F$ .

Here, we focus on a sister compound, cubic  $D0_3$   $\text{Fe}_3\text{Si}$  (Fig.1(a)) [11]. The large ANE in  $\text{Fe}_3\text{Si}$  is predicted by the high throughput calculation [7]. The Curie temperature ( $T_C$ ) of  $\text{Fe}_3\text{Si} \sim 840$  K is higher than that for  $\text{Fe}_3\text{Ga}$  (720 K) and  $\text{Fe}_3\text{Al}$  (600 K) [12–14], which is beneficial for TE application at high temperature. Besides, silicon is the most abundant element in the earth’s crust and widely used for industry. However, the experimental report of ANE for  $\text{Fe}_3\text{Si}$  is limited only for thin films and its value is small  $|S_{yx}| < \sim 1 \mu\text{V/K}$  [15].

In this paper, we report the temperature ( $T$ ) and magnetic field ( $B$ ) dependence of the electric and thermoelectric properties for the bulk polycrystalline  $\text{Fe}_3\text{Si}$ . We find a large room-temperature

---

\* satoru@phys.s.u-tokyo.ac.jp

---

Nernst coefficient  $S_{yx} \sim 2 \mu\text{V/K}$ , which is twice larger than the previous report using thin films [15]. We also estimate the transverse thermoelectric coefficient  $|\alpha_{yx}|$  and found a large room-temperature value  $\sim 3 \text{ Am}^{-1}\text{K}^{-1}$ , suggesting the dominant intrinsic contribution. The analysis of the band structure indicates dispersion-less flat bands on the  $\Gamma$ -X line might have significant contribution to the large ANE response.

## II. EXPERIMENTS AND DISCUSSION

Polycrystalline  $\text{Fe}_3\text{Si}$  samples were synthesized by the melt cooling method in a mono-arc furnace. As-grown samples were used for all characterization and measurements. The powder X-ray diffraction (XRD) result shows the single phase of the  $D0_3$   $\text{Fe}_3\text{Si}$  with a lattice constant of  $5.65 \text{ \AA}$ . The scanning Electron Microscope-Energy Dispersive X-ray Spectrometry (SEM-EDX) method shows our  $\text{Fe}_3\text{Si}$  is stoichiometric within a few percent resolutions. The bar-shaped samples were used for all the transport properties, including Hall and longitudinal resistivity ( $\rho_{yx}$  and  $\rho_{xx}$ ), Nernst and Seebeck coefficients ( $S_{yx}$  and  $S_{xx}$ ) in a physical properties measurement system (PPMS, Quantum Design) with a thermal transport option (TTO). To remove the longitudinal contributions,  $\rho_{xx}$  and  $S_{xx}$ , the temperature dependence of  $\rho_{yx}$  and  $S_{xx}$  were evaluated by symmetrization of the data with the positive and negative field sweeps. Magnetization was measured by a commercial magnetic properties measurement system (MPMS, Quantum Design) with the needle-like sample ( $\sim 0.2 \text{ mg}$ ). For all measurements, no specific orientation was chosen since the poly-crystalline nature could guarantee isotropic transport properties.

The electronic structure of  $\text{Fe}_3\text{Si}$  was obtained by using the OpenMX code [16], where the exchange-correlation functional within the generalized gradient approximation and norm-conserving pseudopotentials were employed [17]. The spin-orbit coupling was induced by using total angular momentum-dependent pseudopotentials. The wave functions were expanded by a linear combination of multiple pseudoatomic orbitals [18]. A set of pseudoatomic orbital basis was specified as  $\text{Fe}5.5\text{-}s3p2d2f1$ ,  $\text{Si}7.0\text{-}s3p3d2$ , where the number after each element stands for the radial cutoff in the unit of Bohr and the integer after  $s$ ,  $p$ ,  $d$ , and  $f$  indicates the radial multiplicity of each angular momentum component. The lattice constant was set to the experimental lattice constant of  $5.65 \text{ \AA}$ . The cutoff energies for a charge density of 500 Ry and a  $k$ -point mesh of  $36 \times 36 \times 36$  were used.

Figure 1(b) shows the magnetic field dependence of magnetization  $M$  at 300 K for  $\text{Fe}_3\text{Si}$  ferro-

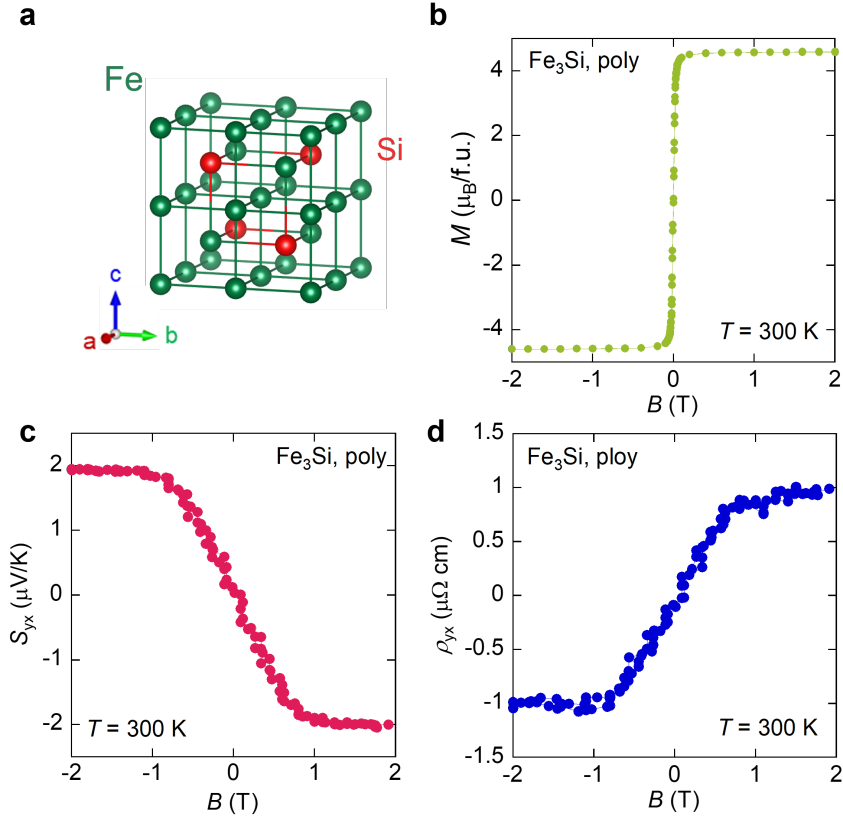


FIG. 1. (Color online) (a) The ordered cubic  $D0_3$  structure for  $\text{Fe}_3\text{Si}$  (Space group:  $Fm\bar{3}m$ ) (b)-(d) The magnetic field dependence of the magnetization  $M$  (b), the Nernst coefficient  $S_{yx}$  (c) and the Hall resistivity  $\rho_{yx}$  (d) for polycrystal  $\text{Fe}_3\text{Si}$  at 300 K.

magnet. The saturated magnetization  $M_s$  is around  $4.6 \mu_B/\text{f.u}$  at 300 K, which is comparable to the previous research ( $M \sim 4.5 \mu_B/\text{f.u}$ ) [19]. As predicted by the Slater-Pauling rule,  $M_s$  for  $\text{Fe}_3\text{Si}$  is smaller than  $\text{Fe}_3\text{Ga}$  and  $\text{Fe}_3\text{Al}$  owing to the smaller number of valence electrons [7]. Figure 1 (c) and (d) show the  $B$  dependence of the Nernst coefficient  $S_{yx}$  and the Hall resistivity  $\rho_{yx}$ , respectively. Both  $S_{yx}$  and  $\rho_{yx}$  saturate at  $B \sim 0.9$  T. The difference between the saturated magnetic field in magnetization ( $M$ ) and transport properties ( $S_{yx}$  and  $\rho_{yx}$ ) originates from the demagnetization effect owing to the shape anisotropy.  $S_{yx}$  reaches  $\sim 2 \mu\text{V/K}$ , which is nearly 10 times larger than that of pure iron [20]. This value is also comparable to the recent topological magnets such as kagome metal  $\text{Fe}_3\text{Sn}$ ,  $\text{Fe}_3\text{Sn}_2$  and  $\text{TbMn}_6\text{Sn}_6$  [21–23], suggesting some topological feature in the band structure may also be important in  $\text{Fe}_3\text{Si}$ .

To understand the mechanism of the large  $S_{yx}$  in  $\text{Fe}_3\text{Si}$ , we also measure  $T$  dependence of both transverse and longitudinal electric ( $\rho_{yx}$  and  $\rho_{xx}$ ) and thermoelectric properties ( $S_{yx}$  and  $S_{xx}$ ) as shown in Fig. 2. On cooling,  $-S_{yx}$  peaks at  $T \sim 340$  K and then monotonically decreases down to the lowest temperature.  $-S_{yx}$  becomes slightly negative below  $\sim 70$  K due to the carrier type change. Similarly, Seebeck coefficient  $S_{xx}$  at zero fields also shows a peak around 340 K and monotonically decreases down to  $\sim 70$  K accompanied by the sign change at  $\sim 160$  K as shown in Fig.2 (c). The sign change of  $S_{xx}$  indicates the change of the dominant carrier type from the electron at high  $T$  to the hole low  $T$ .

On the other hand,  $\rho_{yx}$  monotonically decreases down to the lowest temperature (Fig.2 (b)). Although  $\rho_{yx}$  is governed by the AHE at high temperatures, clear  $B$ -linear ordinary Hall effect (OHE) contribution appears at low temperatures  $T < \sim 100$  K and finally dominates at  $T \sim 2$  K as shown in the inset of Fig.2 (b). As shown in Fig.2 (d),  $T$  dependence of  $\rho_{xx}$  exhibits a typical metallic behavior, monotonically decreasing on cooling to the lowest temperature. Although the residual resistivity ratio (RRR) is similar to  $\text{Fe}_3\text{Ga}$  single crystals, the absolute value of  $\rho_{xx}$  for  $\text{Fe}_3\text{Si}$  is only about 70% of that of  $\text{Fe}_3\text{Ga}$  [7].

To check the intrinsic contribution for ANE and AHE, we experimentally estimate the Hall conductivity  $\sigma_{yx}$  and transverse thermoelectric conductivity  $\alpha_{yx}$  based on the following formulas,

$$\alpha_{yx} = \frac{1}{\rho_{xx}} [S_{yx} - \frac{\rho_{yx}}{\rho_{xx}} S_{xx}], \quad (1a)$$

$$\sigma_{yx} = -\rho_{yx} / \rho_{xx}^2. \quad (1b)$$

The obtained  $-\sigma_{yx}$  and  $-\alpha_{yx}$  are shown in Figs. 3 (a) and 3(b), respectively. Here, we only show the data above  $\sim 100$  K since we cannot easily separate the ordinal Hall/Nernst contribution at low temperatures as discussed above. As shown in Fig. 3 (a),  $-\sigma_{yx}$  shows a broad peak around 300 K and gradually decreases down to 100 K. On the other hand,  $-\alpha_{yx}$  increases to  $3 \text{ Am}^{-1}\text{K}^{-1}$  with a kink at  $T \sim 340$  K and then monotonically decreases on cooling.

The equation (1a) can be rewritten as,

$$S_{yx} = \alpha_{yx}\rho_{xx} - \sigma_{yx}\rho_{xx}S_{xx} \equiv S_1 + S_2, \quad (2)$$

The second term could be also expressed as  $S_2 = -\tan(\theta_{AHE})S_{xx}$ , where  $\tan(\theta_{AHE})$  is anomalous Hall angle. The first term  $S_1$  represents the transverse voltage directly driven by the transverse thermoelectric coefficient  $\alpha_{yx}$  while the second term  $S_2$  can be regarded as the Hall effect of the current flow generated by the Seebeck effect. As shown in Figure 3 (c), the contribution from  $S_2$

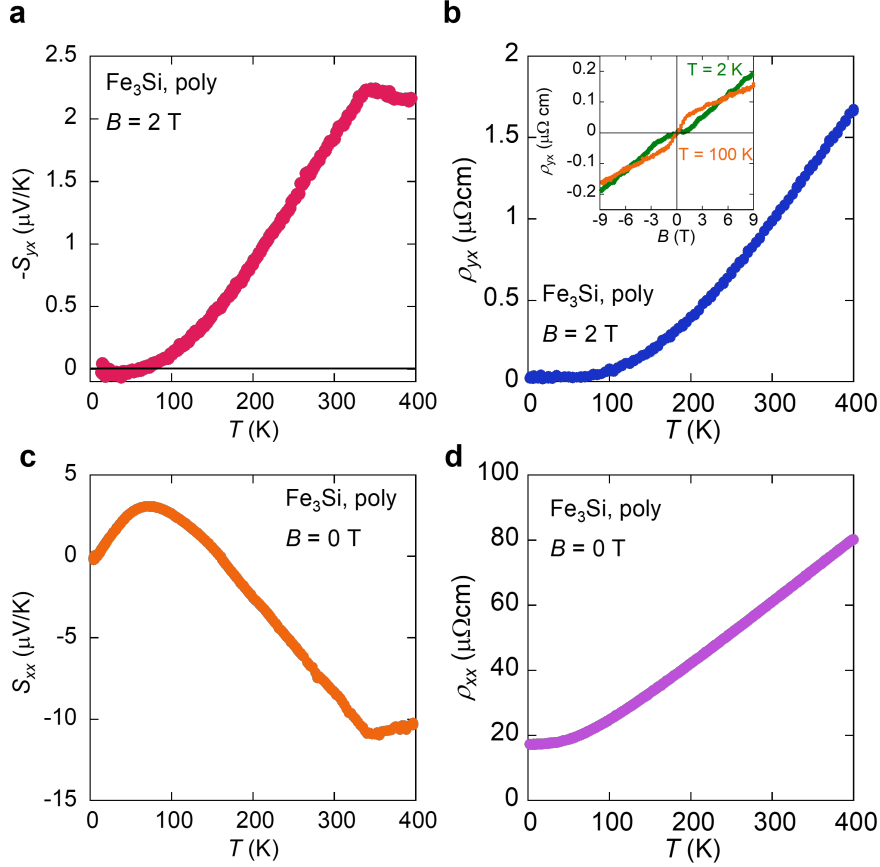


FIG. 2. (Color online) (a, b) The temperature  $T$  dependence of the Nernst coefficient  $-S_{yx}$  (a) and Hall resistivity  $\rho_{yx}$  (b) under the magnetic field of 2 T. The inset of Figure 2 (b) is the field dependence of  $\rho_{yx}$  at 2 K and 100 K. (c, d) The temperature  $T$  dependence of the Seebeck coefficient  $S_{xx}$  (c) and longitudinal resistivity  $\rho_{xx}$  (d) under zero magnetic field.

is almost negligible around room temperature ( $\sim 10\%$  of  $S_1$ ). This indicates that the origin of the large ANE at room  $T$  is indeed the large  $\alpha_{yx}$ .

In fact, the room temperature  $|\alpha_{yx}|$  for Fe<sub>3</sub>Si is even larger than that for some topological materials with large ANE, such as Co<sub>2</sub>MnGa [ $|\alpha_{yx}| \sim 2.7 \text{ Am}^{-1}\text{K}^{-1}$ ] and Fe<sub>3</sub>Sn [ $|\alpha_{yx}| \sim 2.3 \text{ Am}^{-1}\text{K}^{-1}$ ] [8, 22]. However, the experimental  $S_{yx}$  for Fe<sub>3</sub>Si at 300 K is much smaller than Co<sub>2</sub>MnGa [ $S_{yx} \sim 6.5 \text{ μV/K}$ ]. According to equation (2), this difference can be explained by two reasons. Firstly, the  $\rho_{xx}$  for Fe<sub>3</sub>Si is smaller than those topological semimetals [7, 8, 22]. The Nernst voltage is the combination of the current flow induced by spin-orbital coupling (SOC) and

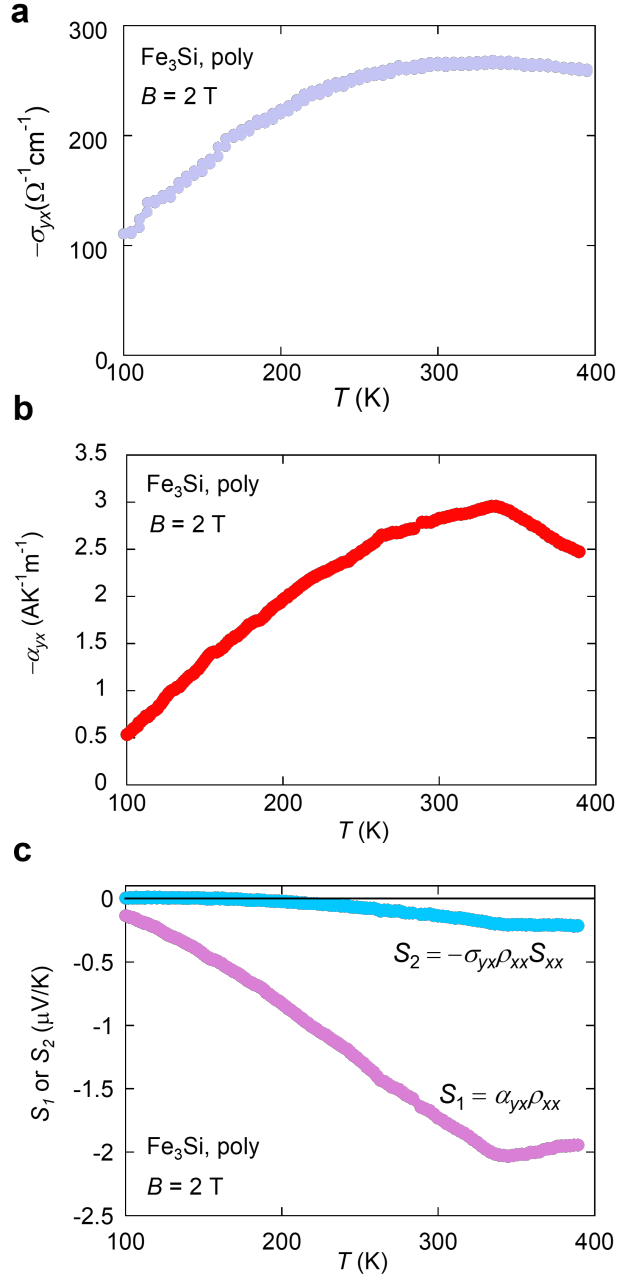


FIG. 3. (Color online) The temperature  $T$  dependence of the Hall conductivity  $-\sigma_{yx}$  (a), the transverse thermoelectric conductivity  $-\alpha_{yx}$  (b), and two contributions  $S_1$  and  $S_2$  to anomalous Nernst effect (c) under the magnetic field of 2 T.

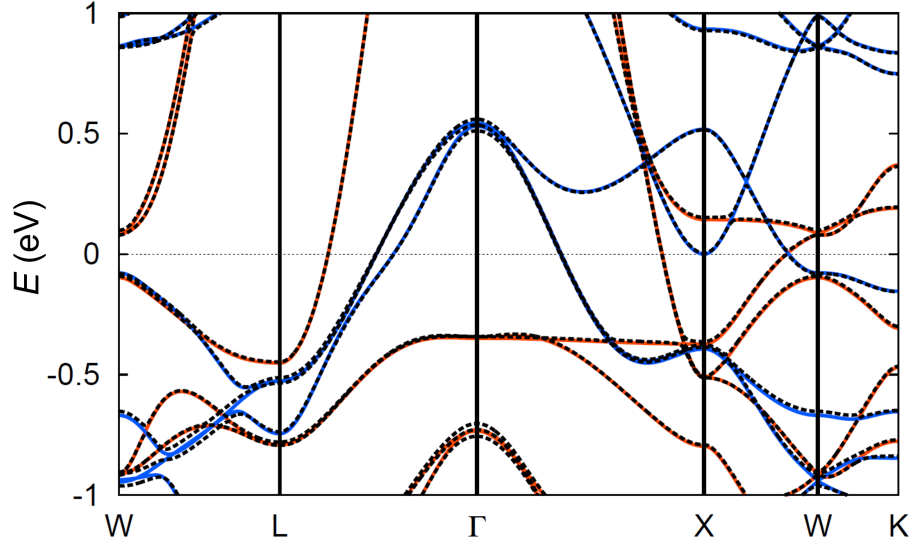


FIG. 4. (Color online) Band structure around the Fermi energy for Fe<sub>3</sub>Si obtained from first-principles calculations for the case of magnetization  $M = 5.1 \mu_B/\text{f.u.}$  along [001]. The red and blue lines represent the majority and minority bands without SOC, respectively. The black dotted line corresponds to the bands with SOC.

the material resistance. Thus, the larger the longitudinal resistivity is, the larger ANE becomes if  $|\alpha_{yx}|$  is the same. However, We note that the large resistivity suppresses the magnitude of the figure of merit  $ZT = \sigma S^2 T / \kappa$ , power factor  $PF = \sigma S^2$  and the specific power generation capacity  $\Gamma_P = P_{\max} / (A (\Delta T)^2)$  in thermoelectric devices. Therefore, semimetals with a resistivity of  $100 \sim 200 \mu\Omega \text{ cm}$  at room temperature are more suitable for practical applications. Secondly, the second term  $S_2$  doesn't contribute too much to the total  $S_{yx}$  in Fe<sub>3</sub>Si. In Co<sub>2</sub>MnGa, this contribution accounts for roughly 50 % of the total  $S_{yx}$  because of the large Hall angle  $\tan(\theta_{AHE})$  [8]. This phenomenon is also found in Co<sub>3</sub>Sn<sub>2</sub>S<sub>2</sub> [9, 24]. In order to utilize  $S_2$  to improve the total  $S_{yx}$ , the  $\tan(\theta_{AHE})$  should be large  $\sim 0.1$ , which is often discovered in topological ferromagnets with Weyl points [25, 26].

Figure 4 shows the band structure around the Fermi energy for Fe<sub>3</sub>Si obtained from first-principles calculation. Around the L point, nodal web structures similar to Fe<sub>3</sub>Ga, composed of minority bands [27], are found around  $E = E_F - 0.6 \text{ eV}$ . Unlike Fe<sub>3</sub>Ga, the distance of the nodal web from  $E_F$  is far to affect the transport properties. It indicates the origin of the large ANE for Fe<sub>3</sub>Si might be different. In fact, we also found a flat band-like structure on the  $\Gamma$ -X line. Since



---

topological flat band structures could also be the source of giant ANE and AHE [28, 29], a further theoretical investigation is required to reveal the origin of the large transverse thermoelectric coefficient.

### III. CONCLUSIONS

We have discovered a large ANE in the polycrystalline  $\text{Fe}_3\text{Si}$ , the sister compound of  $\text{Fe}_3\text{Ga}$  and  $\text{Fe}_3\text{Al}$ . The one-step synthesis method and the low material cost make it the most promising material in the  $\text{Fe}_3X$  system for future applications. In addition, for thin film applications,  $\text{Fe}_3\text{Si}$  could have better compatibility with other silicon-based electronic devices [30]. The electronic band structure for  $\text{Fe}_3\text{Si}$  indicates that the dispersion-less band on the  $\Gamma$ -X line might induce a large Berry curvature instead of the nodal web structure like  $\text{Fe}_3\text{Ga}$ . However, the topological electronic structure as an origin of large ANE in  $\text{Fe}_3\text{Si}$  is still an open question. For this purpose, systematic research based on single-crystal  $\text{Fe}_3\text{Si}$  is also expected in the future.

### ACKNOWLEDGMENTS

This work was partially supported by JST-Mirai Program (JPMJMI20A1), JST-CREST (JPMJCR18T3), New Energy and Industrial Technology Development Organization (NEDO), and JSPS-KAKENHI (JP19H00650, JP20K22479, JP21J22318, JP22K14587). The work at the Institute for Quantum Matter, an Energy Frontier Research Center was funded by DOE, Office of Science, Basic Energy Sciences under Award # DE-SC0019331. The computations in this research were partially carried out using the Fujitsu PRIMERGY CX400M1/CX2550M5 (Oakbridge-CX) in the Information Technology Center, The University of Tokyo. And the use of the facilities of the Materials Design and Characterization Laboratory at the Institute for Solid State Physics, The University of Tokyo, is gratefully acknowledged.

- 
- [1] Q. Zhang, K. Deng, L. Wilkens, H. Reith, and K. Nielsch, *Nature Electronics* **5**, 333 (2022).
  - [2] N. Jaziri, A. Boughamoura, J. Müller, B. Mezghani, F. Tounsi, and M. Ismail, *Energy Reports* **6**, 264 (2020).
  - [3] L. E. Bell, *Science* **321**, 1457 (2008).

- 
- [4] S. Nakatsuji and R. Arita, *Annual Review of Condensed Matter Physics* **13**, 119 (2022).
- [5] K.-i. Uchida, W. Zhou, and Y. Sakuraba, *Applied Physics Letters* **118**, 140504 (2021).
- [6] M. Ikhlas, T. Tomita, T. Koretsune, M.-T. Suzuki, D. Nishio-Hamane, R. Arita, Y. Otani, and S. Nakatsuji, *Nature Physics* **13**, 1085 (2017).
- [7] A. Sakai, S. Minami, T. Koretsune, T. Chen, T. Higo, Y. Wang, T. Nomoto, M. Hirayama, S. Miwa, D. Nishio-Hamane, *et al.*, *Nature* **581**, 53 (2020).
- [8] A. Sakai, Y. P. Mizuta, A. A. Nugroho, R. Sihombing, T. Koretsune, M.-T. Suzuki, N. Takemori, R. Ishii, D. Nishio-Hamane, R. Arita, *et al.*, *Nature Physics* **14**, 1119 (2018).
- [9] S. N. Guin, P. Vir, Y. Zhang, N. Kumar, S. J. Watzman, C. Fu, E. Liu, K. Manna, W. Schnelle, J. Gooth, *et al.*, *Advanced Materials* **31**, 1806622 (2019).
- [10] Y. Pan, C. Le, B. He, S. J. Watzman, M. Yao, J. Gooth, J. P. Heremans, Y. Sun, and C. Felser, *Nature materials* **21**, 203 (2022).
- [11] R. Ma, Q. Xie, J. Huang, W. Yan, and X. Guo, *Journal of alloys and compounds* **552**, 324 (2013).
- [12] V. Niculescu, K. Raj, J. Budnick, T. Burch, W. Hines, and A. Menotti, *Physical Review B* **14**, 4160 (1976).
- [13] N. Kawamiya, K. Adachi, and Y. Nakamura, *Journal of the Physical Society of Japan* **33**, 1318 (1972).
- [14] T. Shinohara, *Journal of the Physical Society of Japan* **19**, 51 (1964).
- [15] Y. Hamada, Y. Kurokawa, T. Yamauchi, H. Hanamoto, and H. Yuasa, *Applied Physics Letters* **119**, 152404 (2021).
- [16] Openmx: Open source package for material explorer, <http://www.openmx-square.org/>.
- [17] I. Morrison, D. M. Bylander, and L. Kleinman, *Phys. Rev. B* **47**, 6728 (1993).
- [18] G. Theurich and N. A. Hill, *Phys. Rev. B* **64**, 073106 (2001).
- [19] T. Shinjo, Y. Nakamura, and N. Shikazono, *Journal of the Physical Society of Japan* **18**, 797 (1963).
- [20] S. J. Watzman, R. A. Duine, Y. Tserkovnyak, S. R. Boona, H. Jin, A. Prakash, Y. Zheng, and J. P. Heremans, *Physical Review B* **94**, 144407 (2016).
- [21] H. Zhang, C. Xu, and X. Ke, *Physical Review B* **103**, L201101 (2021).
- [22] T. Chen, S. Minami, A. Sakai, Y. Wang, Z. Feng, T. Nomoto, M. Hirayama, R. Ishii, T. Koretsune, R. Arita, *et al.*, *Science advances* **8**, eabk1480 (2022).
- [23] H. Zhang, J. Koo, C. Xu, M. Sretenovic, B. Yan, and X. Ke, *Nature communications* **13**, 1 (2022).
- [24] E. Liu, Y. Sun, N. Kumar, L. Muechler, A. Sun, L. Jiao, S.-Y. Yang, D. Liu, A. Liang, Q. Xu, *et al.*, *Nature physics* **14**, 1125 (2018).

- 
- [25] P. Li, J. Koo, W. Ning, J. Li, L. Miao, L. Min, Y. Zhu, Y. Wang, N. Alem, C.-X. Liu, *et al.*, *Nature communications* **11**, 1 (2020).
- [26] N. Armitage, E. Mele, and A. Vishwanath, *Reviews of Modern Physics* **90**, 015001 (2018).
- [27] S. Minami, F. Ishii, M. Hirayama, T. Nomoto, T. Koretsune, and R. Arita, *Phys. Rev. B* **102**, 205128 (2020).
- [28] Y. D. Kato, Y. Okamura, S. Minami, R. Fujimura, M. Mogi, R. Yoshimi, A. Tsukazaki, K. S. Takahashi, M. Kawasaki, R. Arita, *et al.*, *npj Quantum Materials* **7**, 1 (2022).
- [29] S. Roychowdhury, A. M. Ochs, S. N. Guin, K. Samanta, J. Noky, C. Shekhar, M. G. Vergniory, J. E. Goldberger, and C. Felser, *Advanced Materials* **34**, 2201350 (2022).
- [30] W. Hines, A. Menotti, J. Budnick, T. Burch, T. Litrenta, V. Niculescu, and K. Raj, *Physical Review B* **13**, 4060 (1976).